Astronomy & Astrophysics manuscript no. article˙v3
February 28, 2013

Statistical seismology of transverse waves in the solar corona

E. Verwichte[1,2], T. Van Doorsselaere[2], R. S. White[1], and P. Antolin[2]

[1] Department of Physics, University of Warwick, Coventry CV4 7AL, UK
e-mail: Erwin.Verwichte@warwick.ac.uk
[2] Centre for Plasma Astrophysics, Department of Mathematics, Katholieke Universiteit Leuven, Celestijnenlaan 200B, 3001 Leuven, Belgium

ABSTRACT

Context. Observations show that transverse oscillations occur commonly in solar coronal loops. The rapid damping of these waves has been attributed to resonant absorption. The oscillation characteristics carries information of the structuring of the corona. However, self-consistent seismological methods to extract information from individual oscillations is limited because there are less observables than model unknown parameters and the problem is underdetermined. Furthermore, it has been shown that one-to-one comparisons of the observed scaling of period and damping times with wave damping theories is misleading.
Aims. We aim to investigate if seismological information can be gained from the observed scaling laws in a statistical sense.
Methods. A statistical approach is used whereby scaling-laws are produced by forward modelling using distributions of values for key loop cross-sectional structuring parameters. We study two types of observations: 1) transverse loops oscillations as seen mainly with TRACE and SDO and 2) running transverse waves seen with CoMP.
Results. We demonstrate that the observed period-damping time scaling law does provide information about the physical damping mechanism, if observations are collected from as wide as possible range of periods and a comparison with theory is performed in a statistical sense. The distribution of the ratio of damping time over period, i.e. the quality factor, has been derived analytically and fitted to the observations. A minimum value for the quality factor of 0.65 has been found. From this, a constraint linking the ranges of possible values for the density contrast and inhomogeneity layer thickness is obtained for transverse loop oscillations. If the layer thickness is not constrained, then the density contrast is maximally equal to 3. For transverse waves seen by CoMP, it is found that the ratio of maximum to minimum values for these two parameters has to be less than 2.06. i.e. the sampled values for the layer thickness and Alfvén travel time comes from a relatively narrow distribution.
Conclusions. Now that more and more transverse loop oscillations have been analysed, a statistical approach to coronal seismology becomes possible. Using the observed data cloud restrictions in the loop parameter space of density contrast and inhomogeneity layer thickness are found and surprisingly for the running waves narrow distributions for loop parameters have been found.

Key words. Sun:oscillations – Magnetohydrodynamics (MHD)

1. Introduction

Transverse waves are pervasive in the solar corona. They have been detected with confidence since 1998 (Aschwanden et al. 1999; Nakariakov et al. 1999) in the form of transverse loop oscillations (TLOs). To date, more than 50 TLOs have been reported with periods ranging between 100s and 3 hours (Aschwanden et al. 2002; Wang & Solanki 2004; Verwichte et al. 2004; Hori et al. 2005, 2007; Van Doorsselaere et al. 2007; De Moortel & Brady 2007; Van Doorsselaere et al. 2009; Verwichte et al. 2009, 2010; Mrozek 2011; White & Verwichte 2012; White et al. 2012; Verwichte et al. 2012). The majority of these oscillations have been studied using EUV imagers such as TRACE (Handy et al. 1999), EUVI/STEREO (Howard et al. 2008) and AIA/SDO (Lemen et al. 2012). They are reported to damp quickly with oscillation quality factors in the range 0.6-5.4.

Tomczyk et al. (2007) demonstrated using ground-based spectral measurements with the Coronal Multichannel Polarimeter (CoMP) (Tomczyk et al. 2008) that small-amplitude propagating transverse waves are ubiquitous in the solar corona. This result seems to be supported by the recent report of running transverse waves in coronal loops by AIA/SDO (McIntosh et al. 2011; Wang et al. 2012).

A widely accepted explanation for the rapid damping is the mechanism of resonant absorption where the transverse wave is considered to be an Alfvénic kink mode (or surface Alfvén mode Wentzel 1979; Goossens et al. 2012) whose nature evolves, through a resonance at a loop layer where its frequency matches the local Alfvén frequency, from a global transverse loop motion to a local mainly azimuthal motion (Ruderman & Roberts 2002; Goossens et al. 2002). Once local, the mode cannot be observed directly and it then proceeds to damp dissipatively enhanced by phase-mixing (or alternatively collisionlessly). Crucially it is the rate of mode evolution from global to local that is observed as the rapid damping of the transverse wave. The observed damping time depends on the structure of the Alfvén frequency across the loop.

Hence, besides the loop's average Alfvén speed and magnetic field strength (Nakariakov & Ofman 2001), there is the potential for seismologically determining the loop cross-section profile, including the density contrast, which are difficult to measure directly (e.g. Aschwanden et al. 2003; Schmelz et al. 2003; Terzo & Reale 2010). By combining the theories for the propagation and damping of the transverse wave it is possible to constrain self-consistently the unknown parameters in the problem (Verwichte et al. 2006). However, for the resonant absorption damping model, the problem is under-determined and it is not possible to deduce both density contrast and inhomogene-

ity layer thickness independently (Arregui et al. 2007; Goossens et al. 2008; Arregui & Asensio Ramos 2011).

Ofman & Aschwanden (2002) modelled the scaling relations, e.g. between damping time and period, for different damping mechanisms. They found that the observed scaling relations were more compatible with phase mixing. However, it was pointed out by Arregui et al. (2008) that a one-to-one comparison between the observed scaling and the linear scaling from resonant absorption inherently makes the unrealistic assumption that all loops have the same cross-sectional structuring. In fact, by allowing the cross-sectional profile to vary between events, they showed that the scaling from resonant absorption can easily depart from linear. Thus, they concluded that scaling laws were not sufficient to distinguish damping mechanisms, because resonant absorption can reproduce several dependencies using carefully chosen distributions of equilibrium parameters. However, now it becomes possible to use the inverse approach. Since 2002 (Aschwanden et al. 2002), the number of observations and the range of observed periods has increased. Given the observed scaling laws of periods and damping time, can we find information on the statistical distributions of equilibrium parameters of coronal loops that exist in the solar corona? In this article we will show that it is possible to use statistical and forward-modelling approaches to model scaling laws of loops. This statistical, seismological information on the coronal loop ensemble can potentially help to distinguish between different coronal loop models and heating mechanisms.

The paper is structured in two main parts. Section 2 investigates statistically the scaling of TLOs using two approaches. Section 3 studies statistically the transverse waves seen by CoMP (Tomczyk et al. 2007). We discuss our findings in Sect. 4.

2. Statistics of transverse loop oscillations

Since 2002, when Ofman & Aschwanden (2002) modelled the scaling relations for standing transverse loop oscillations (TLOs), many more observations have been analysed. Table 1 lists 52 events of TLOs from 13 studies. Figure 1 shows the distribution of damping times, τ, versus oscillation period, P. We can find a power-law relationship between those two observed quantities as

$$\tau = \alpha P^{\gamma} \ , \ \log_{10}\alpha = 0.44 \pm 0.31 \ , \ \gamma = 0.94 \pm 0.12 \ . \quad (1)$$

Under the assumption of a loop where the density drops from inner to external conditions over a thin transition layer, the resonant absorption rate is given by (e.g. Ionson 1978; Hollweg & Yang 1988; Goossens et al. 1992; Ruderman & Roberts 2002)

$$\tau = \xi_{\rm E} \ P \ , \ \xi_{\rm E}(\ell/a, \zeta) = F\,(\ell/a)^{-1}\,\frac{\zeta+1}{\zeta-1} \ , \quad (2)$$

where F, ℓ, a and ζ are parameters that describe the cross-sectional profile of the loop mass density, $\rho(r)$. Here, we choose a half-wavelength sinusoidally varying transition layer, i.e.

$$\frac{\rho(r)}{\rho_i} = \begin{cases} 1 & r-a < -\ell/2 \\ \frac{1}{2}\left[(\zeta^{-1}+1)+(\zeta^{-1}-1)\,\sin\frac{\pi(r-a)}{\ell}\right] & |r-a| \le \ \ell/2 \\ \zeta^{-1} & r-a > \ \ell/2 \end{cases} , \quad (3)$$

where ρ_i is the loop-axis equilibrium density and ζ is the ratio of the loop-axis density over the external density, i.e. $\zeta{=}\rho_i/\rho_e$. For such a profile, $F = 2/\pi$. Equation (2) is strictly speaking only valid in the regime where $\ell \ll a$, though Van Doorsselaere et al. (2004) showed that it still provides a relatively accurate extension into the regime of finite resonance layer widths. Also, Eq. (2) does not describe any transient behaviour in the damping (Pascoe et al. 2012).

Equation (2) shows that the resonant absorption time-scale scales linearly with period. This matches well with the observed scaling. However, as pointed out by Arregui et al. (2008), a one-to-one comparison is problematic because Eq. (2) also depends on ℓ/a and ζ, which will vary between loops. We can identify the

Table 1. Characteristics of observed TLOs

#	P (s)	τ (s)	L (Mm)	Reference[(1)]
1	261	870	168	A02
2	265	300	72	
3	316	500	174	
4	277	400	204	
5	272	849	162	
6	435	600	258	
7	143	200	166	
8	423	800	406	
9	185	200	192	
10	396	400	146	
11	234	714	350 ± 50	WS04
12	249 ± 33	920 ± 360	218	V04
13	448 ± 18	1260 ± 500	218	
14	392 ± 31	1830 ± 790	228	
15	382 ± 12	1330 ± 528	233	
16	358 ± 30	1030 ± 570	237	
17	326 ± 45	980 ± 400	235	
18	357 ± 89	1320 ± 720	236	
19	567	1500	400 ± 100	H05 & H07
20	918	4200	800 ± 200	
21	425	2300	384	VD07
22	436 ± 4.5	2129 ± 280	400 ± 40	
23	243 ± 6.4	1200	400 ± 40	
24	895 ± 2	521 ± 8	228	DMB07 & VD09
25	452 ± 1	473 ± 6	228	
26	630 ± 30	1000 ± 300	340 ± 15	V09
27	2418 ± 5	3660 ± 80	680 ± 50	V10
28	377	500	250	M11
29	225 ± 40	240 ± 45	121 ± 12	WV12
30	215 ± 5	293 ± 18	111 ± 11	
31	213 ± 9	251 ± 36	132 ± 13	
32	216 ± 27	230 ± 23	113 ± 11	
33	520 ± 5	735 ± 53	396 ± 40	
34	596 ± 50	771 ± 336	374 ± 37	
35	212 ± 20	298 ± 30	279 ± 28	
36	256 ± 22	444 ± 105	240 ± 24	
37	135 ± 9	311 ± 85	241 ± 24	
38	115 ± 2	175 ± 30	159 ± 16	
39	103 ± 8	242 ± 114	132 ± 13	
40	302 ± 14	306 ± 43	466 ± 50	W12
41	565 ± 4	666 ± 42	301 ± 30	V12
42	222 ± 18	420 ± 360	274 ± 30	
43	474 ± 12	900 ± 120	400 ± 30	
44	1170 ± 6	1218 ± 48	400 ± 30	
45	623 ± 4	960 ± 60	270 ± 30	
46	150 ± 5	216 ± 60	188 ± 20	
47	122 ± 6	348 ± 360	160 ± 20	
48	273 ± 54	468 ± 36	171 ± 20	
49	282 ± 6	606 ± 186	122 ± 20	
50	491 ± 18	834 ± 6	262 ± 20	
51	348 ± 7	906 ± 288	238 ± 20	
52	340 ± 3	930 ± 144	200 ± 20	

[(1)] The reference citations are listed in Fig. 1

observed fit parameter α with $\xi_E(\ell/a, \zeta)$. What possible range of values of ℓ/a and ζ gives the best match between α and ξ_E?

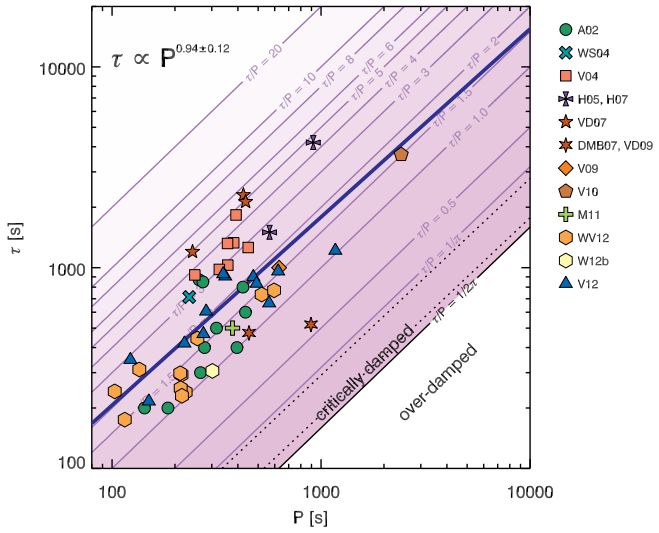

Fig. 1. Damping time versus period of measured TLOs. The thick line is a power-law fit of the form $\tau = \alpha\, P^{\gamma}$. The parallel lines indicate contours of quality factor τ/P. The symbols correspond to the following publications reporting TLOs. A02: Aschwanden et al. (2002), WS04: Wang & Solanki (2004), V04: Verwichte et al. (2004), H05: Hori et al. (2005), H07: Hori et al. (2007), VD07: Van Doorsselaere et al. (2007), DMB07: De Moortel & Brady (2007), VD09: Van Doorsselaere et al. (2009), V09: Verwichte et al. (2009), V10: Verwichte et al. (2010), M11: Mrozek (2011), WV12: White & Verwichte (2012), W12: White et al. (2012), V12: Verwichte et al. (2012).

2.1. Modelling of the damping time-period scaling

In order to make a comparison between theoretical and observed scaling, the following forward-modelling procedure is adopted. The hidden variables are allowed to have a distribution of plausible values and are assumed to be independent. The distribution of the thickness of the inhomogeneity layer, ℓ/a, and the density contrast, ζ, are modelled as

$$\begin{aligned} \frac{\mathrm{d}(\ell/a)}{\mathrm{d}N} &= H(\ell/a, (\ell/a)_{\min}, (\ell/a)_{\max}) \,, \\ \frac{\mathrm{d}\zeta}{\mathrm{d}N} &= H(\zeta, \zeta_{\min}, \zeta_{\max}) \,, \end{aligned} \tag{4}$$

where $H(x, x_{\min}, x_{\max})$ is the top-hat function defined as

$$H(x, x_{\min}, x_{\max}) = \begin{cases} (x_{\max} - x_{\min})^{-1} & x_{\min} \le x \le x_{\max} \\ 0 & x < x_{\min} \text{ or } x > x_{\max} \end{cases} . \tag{5}$$

Alternatively, for ζ, we may also use a Jeffrey's probability density function, $J(x)$, which is defined as

$$J(x, x_{\min}, x_{\max}) = \left[x \ln\left(\frac{x_{\max}}{x_{\min}}\right)\right]^{-1} . \tag{6}$$

Inherently, the distributions do not depend on other physical parameters or on the period. Thus, we make the assumption that the distribution of these parameters is the same for all sizes of loops. Also, the oscillation period has a distribution

$$\frac{\mathrm{d}\log_{10} P}{\mathrm{d}N} = H(\log_{10} P, \log_{10} P_{\max}, \log_{10} P_{\min}) \,, \tag{7}$$

with $P_{\min} = 50$ s and $P_{\max} = 3600$ s, chosen to reflect the bias of observers to identify and study oscillations in the range of several minutes.

There are M number of observations of TLOs. We thus sample M values from these distributions to produce M sets of values $((\ell/a)_i, \zeta_i, P_i)$, $i \in [1, M]$. Using Eq. (2), the corresponding values of τ_i are calculated. Figure 2 shows an example of a realisation. Then, a power-law as Eq. (1) is fitted to this realisation of M pairs of values (P_i, τ_i) and α and γ determined. This process is repeated to produce N realisations of α and γ. The distribution of α and γ, it's mean and standard deviation, are then compared with the observations. Figure 3 shows how the forward-modelled distribution of the observed scaling parameters α and γ match the observed values well with similar uncertainties. The same conclusions can be drawn when using a Jeffrey's distribution for ζ.

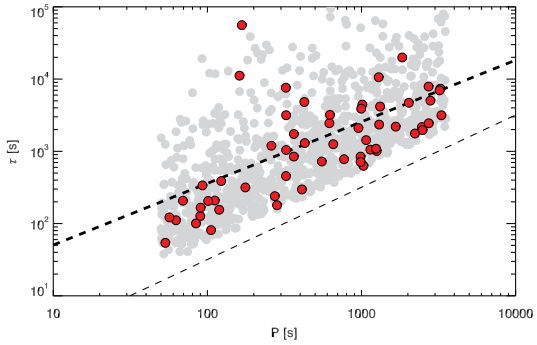

Fig. 2. An example of a realisation of a set of forward-modelled set of (P_i, τ_i) of the same number as currently reported TLOs. The grey circles indicate a realisation of a 1000 sets. Here, ζ and ℓ/a are sampled uniformly from the intervals [0,4] and [0,2], respectively.

Now we wish to investigate if, by optimising the fit between forward modelled and observed distribution, we can constrain the intervals of ζ and ℓ/a and hence extract seismologically information about the transverse structuring of the oscillating loops. Unfortunately, because the spread of α is large, it is difficult to constrain both hidden variables. Therefore, we decide to fix ℓ/a to always be sampled uniformly from the interval [0,2]. We also fix $\zeta_{\min}$ to be unity. Thus, the only remaining free parameter is $\zeta_{\max}$. For each value of $\zeta_{\max}$ we compute a forward-modelled distribution and find its scaling parameters. Figure 4 shows how the forward-modelled value of α varies as a function of $\zeta_{\max}$. Though the error bars are quite large, we can identify the optimal value $\zeta_{\max} = 3$ and that most likely ζ lies in the range [1,10].

2.2. The quality-factor probability density distribution

We use a second method to constrain ℓ/a and ζ by considering the distribution of the quality factor. As Fig. 2 illustrates, a set of values sampled from the distributions in ℓ/a and ζ, and using Eq. (2), leads to a non-uniform spread of values in the P-τ parameter space. We derive analytically this distribution from the distributions of ℓ/a and ζ. We make use of the following relations for distributions of dimensionless quantities x, y and z where the relations $y = y(x)$ and $z = xy$ are monotonic:

$$\frac{\mathrm{d}y}{\mathrm{d}N} = \left|\frac{\mathrm{d}x(y)}{\mathrm{d}y}\right| \frac{\mathrm{d}x}{\mathrm{d}N} \,, \quad \frac{\mathrm{d}z}{\mathrm{d}N} = \int_{-\infty}^{+\infty} \frac{\mathrm{d}x}{\mathrm{d}N} \frac{\mathrm{d}(z/x)}{\mathrm{d}N} \frac{\mathrm{d}x}{|x|} \,. \tag{8}$$

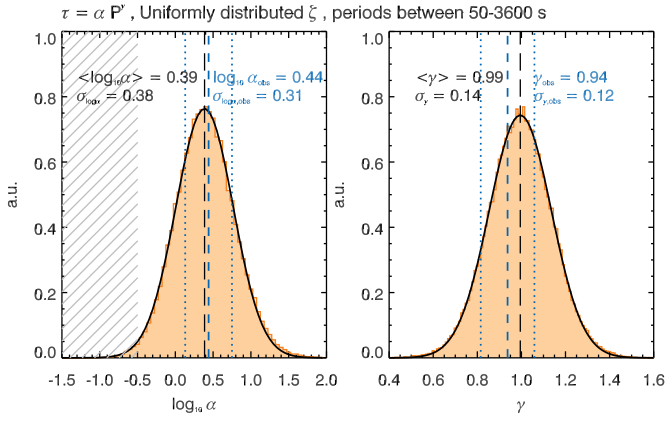

Fig. 3. Forward modelling of power law for resonant absorption model with uniform distributions. ℓ/a and ζ are sampled uniformly from the intervals [0,2] and [0,4], respectively. The hatched region denoted values of α less than $F/2$, which Eq. (2) does not permit.

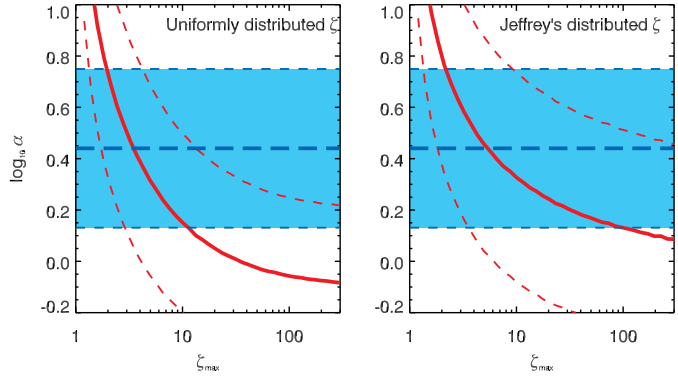

Fig. 4. The mean parameter $\log_{10}\alpha$ as a function of $\zeta_{\max}$ with $\zeta_{\min} = 1$ obtained from N fits to a forward modelled sample of values of periods and damping times, using the uniform distribution for ℓ/a given in Eq. (4) and a uniform (Left) and a Jeffrey's (Right) distributions for ζ as given in Eqs. (4) and (6), respectively. The dashed curves bound the one-σ variation in $\log_{10}\alpha$. The horizontal long-dashed line shows the observed value of $\log_{10}\alpha$ bounded by its one-σ variation.

We introduce the notations $h(\zeta) = (\zeta+1)/(\zeta-1)$, $y = F(\ell/a)^{-1}$ and $q = \tau/P$ for the inverse Atwood number, inverse inhomogeneity scale-length and quality factor, respectively (The function $h(\zeta)$ is shown in Fig. 6). Equation (2) then simply reads $q = y\,h$. We find for uniform distributions of ℓ/a and ζ

$$\frac{\mathrm{d}y}{\mathrm{d}N} = \frac{1}{y^2} H\left(y, F(\ell/a)^{-1}_{\max}, F(\ell/a)^{-1}_{\min}\right) , \quad (9)$$

$$\frac{\mathrm{d}h}{\mathrm{d}N} = \frac{2}{(h-1)^2} H\left(h, h(\zeta_{\max}), h(\zeta_{\min})\right) ,$$

$$= \frac{2y^2}{(y-q)^2} H\left(y, \frac{q}{h(\zeta_{\min})}, \frac{q}{h(\zeta_{\max})}\right) . \quad (10)$$

Using the formula for the product of two distributions (8), the distribution for the quality factor becomes of the form

$$\frac{\mathrm{d}q}{\mathrm{d}N} \propto \int_{y_{\min}}^{y_{\max}} \frac{\mathrm{d}y}{y(y-q)^2} = q^{-2}\,\phi(q) , \quad (11)$$

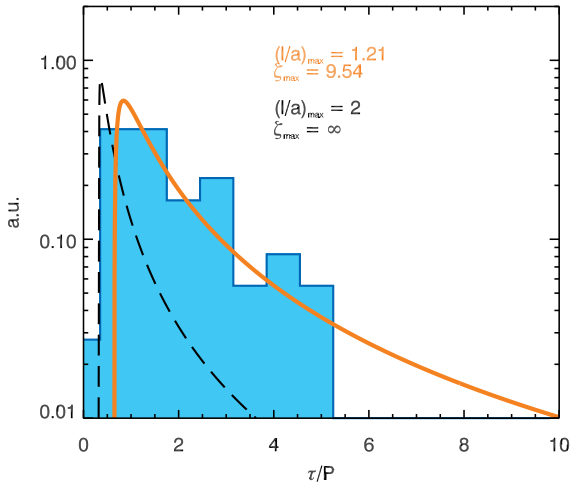

Fig. 5. Distribution of quality-factor, τ/P, from the observations (rough, blue distribution) and from the analytical distribution using Eq. (11) with $\ell/a_{\max} = 1.2$ and $\zeta_{\max} = 9.5$.

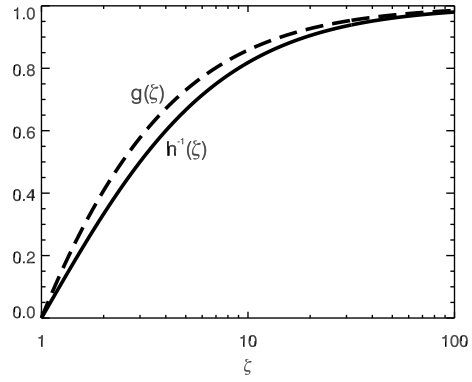

Fig. 6. The dependence of $h^{-1}(\zeta)$ and $g(\zeta)$ on ζ.

where $\phi(q)$ contains the details of the ranges of values of ℓ/a and ζ,

$$\phi(q, (\ell/a)_{\min}, (\ell/a)_{\max}, \zeta_{\min}, \zeta_{\max}) = \left[\frac{q}{q-y} + \ln\left|\frac{y}{q-y}\right|\right]_{y_{\min}}^{y_{\max}} , \quad (12)$$

and with

$$y_{\min} = \max\left(\frac{F}{(\ell/a)_{\max}}, \frac{q}{h(\zeta_{\min})}\right) ,$$

$$y_{\max} = \min\left(\frac{F}{(\ell/a)_{\min}}, \frac{q}{h(\zeta_{\max})}\right) . \quad (13)$$

When ζ is Jeffrey's distributed, we find the same result as above except that the logarithmic terms in ϕ are absent. Equation (12) is simplified if we take the reasonable choices $(\ell/a)_{\min} = 0$ and $\zeta_{\min} = 1$. With $y_{\min} = F/(\ell/a)_{\max}$ and $y_{\max} = q/h(\zeta_{\max})$ Eq. (12) reduces to

$$\phi(q, (\ell/a)_{\max}, \zeta_{\max}) = \frac{h(\zeta_{\max})}{h(\zeta_{\max})-1} - \ln|h(\zeta_{\max})-1|$$

$$- \frac{q\,(\ell/a)_{\max}}{q\,(\ell/a)_{\max} - F} - \ln\left|\frac{F}{q(\ell/a)_{\max} - F}\right| \quad (14)$$

Note that the distribution is only physical for τ/P above a lower threshold value, $(\tau/P)_{\rm min}$, which occurs where $y_{\rm min} = y_{\rm max}$, or

$$(\tau/P)_{\rm min} = \frac{F\, h(\zeta_{\rm max})}{(\ell/a)_{\rm max}} \ . \qquad (15)$$

It can easily be seen from Eq. (14) that ϕ has a root at that value. For ℓ/a and ζ taken from the broadest ranges of [0,2] and [1,∞[, ϕ becomes constant almost everywhere, except near $(\tau/P)_{\rm min} = F/2$ where the distribution drops to zero. For that case the distribution scales as $(\tau/P)^{-2}$. The existence of a minimum threshold in the quality factor has been discussed by Goossens et al. (2008) in the context of individual oscillations.

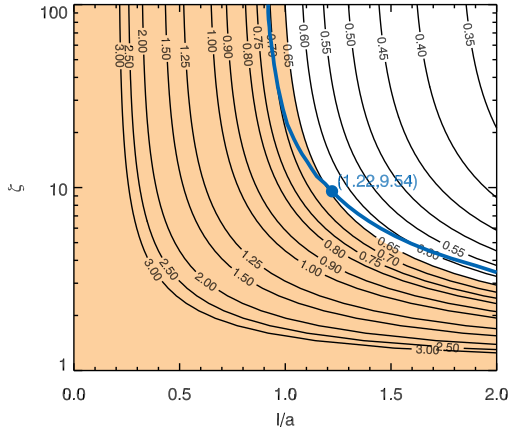

Fig. 7. The allowed range of ℓ/a and ζ for a range of values of $(\tau/P)_{\rm min}$ as derived using Eq. (15). The ranges exist to the left of each curve as illustrated with the shaded area for $(\tau/P)_{\rm min} = 0.65$. The thick curve represents the value of $\zeta_{\rm max}$ as a function of $(\ell/a)_{\rm max}$ that fits best the observed quality factor distribution. A uniform distribution in ζ has been assumed. The use of a Jeffrey's distribution instead would yield an almost identical curve. The dot indicates the values of $(\ell/a)_{\rm max}$ and $\zeta_{\rm max}$ for the fit with the smallest χ^2.

From inspection of the quality factor values of the observations in Fig. 1, one may deduce that expect for one all observations have $\tau/P \geq 1$ (There is one observation with a smaller quality factor but the damping rate has a high uncertainty, Van Doorsselaere et al. 2009). However, an estimate of $(\tau/P)_{\rm min}$ based upon the observed lower limit in τ/P relies on only a few measurements. Instead, we make use of all measurements and fit the observed distribution with Eq. (11) with an arbitrary amplitude and with fixed values of $(\ell/a)_{\rm min} = 0$ and $\zeta_{\rm min} = 1$. As a function of $(\ell/a)_{\rm max}$, we determine from the fit the best value of $\zeta_{\rm max}$. Figure 7 shows this fit as well as the contours of $(\tau/P)_{\rm min}$, calculated from Eq. (15). It approximately follows the contour of constant $(\tau/P)_{\rm min} = 0.65$. Overall, the best fit is for $\ell/a = 1.2$ and $\zeta_{\rm max} = 9.5$ (illustrated in Fig. 5). Then, using Eq. (15) and the value of $(\tau/P)_{\rm min} = 0.65$, we find the constraints

$$2.9 \leq \zeta_{\rm max} = \frac{(\ell/a)_{\rm max} + 0.98}{(\ell/a)_{\rm max} - 0.98} < \infty \ ,$$
$$0.98 \leq (\ell/a)_{\rm max} \leq 2 \ . \qquad (16)$$

For $(\ell/a)_{\rm max} = 2$, ζ is constrained to lie in the interval [1,2.9]. This result is consistent with what was found in the previous subsection. Figure 7 shows that loops with simultaneously large values of ℓ/a and ζ, i.e. smooth and large contrasted loops, are not consistent with the observations.

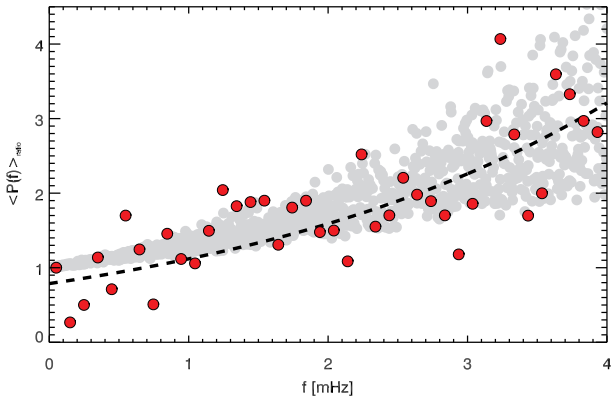

Fig. 8. The CoMP power ratio of downward propagating to upward propagating waves versus the frequency (as taken from Verth et al. 2010) are displayed with red circles. A realisation from 1000 samples from the statistical distributions for $V_{\rm A,i} \in$ [800,1000] km/s, $\ell/a \in$ [0.5,1], $\zeta \in$ [2.5,4] are shown as grey circles. The best fit to the observations, Eq. (21), is shown as the dashed line.

3. Statistics of transverse waves seen by CoMP

Let us now turn our attention to the propagating transverse waves observed by CoMP (Tomczyk et al. 2007; McIntosh et al. 2008), and also by SDO/AIA (McIntosh et al. 2011). We interpret the spatial damping as attenuation due to resonant absorption (Verth et al. 2010; Terradas et al. 2010). As in the previous section, we want to perform seismology on the CoMP data in a statistical sense, by fitting the data using statistical distributions for the loop cross-sectional equilibrium parameters, i.e. the density contrast ζ and the thickness of the smooth layer ℓ/a, and the internal Alfvén transit time $\tau_{\rm A,i}$.

The data we study is displayed in Fig. 2 of Verth et al. (2010) (also as red circles in Fig. 8). They show the ratio of downward propagating wave power (measured as Doppler shifts) with the upward propagating wave power versus the wave frequency. The data is obtained from the $k-\omega$ diagram for CoMP Doppler shifts (McIntosh et al. 2008). In the work of Verth et al. (2010), it is explained that the frequency-dependent power ratio can easily be explained by resonant absorption. In contrast to the previous section with the standing transverse oscillations, the damping for these driven waves is acting as the waves travel along the loop, rather than a temporal damping of the standing transverse waves.

The waves travel at the phase speed, $v_{\rm ph}$, which equals the kink speed (Edwin & Roberts 1983) in the thin loop limit. In the zero plasma-β limit, $v_{\rm ph}$ is thus given by

$$v_{\rm ph} = B\sqrt{\frac{2}{\mu_{\rm o}(\rho_{\rm i}+\rho_{\rm e})}} = V_{\rm A,i}\sqrt{\frac{2\zeta}{\zeta+1}}, \qquad (17)$$

where we have defined $V_{\rm A,i}$ as the loop Alfvén speed. Using Eq. (17), we can now compute the frequency dependence of the power ratio (using Eq. 7 in Verth et al. 2010):

$$<P(f)>_{\rm ratio} = \frac{P_{\rm out}(f)}{P_{\rm in}(f)}\ \exp\left(\mathbb{T}\, f\right) \ , \qquad (18)$$

with

$$\mathbb{T}(\ell/a,\zeta,V_{\rm A,i}) = \frac{2L}{v_{\rm ph}\,\xi_{\rm E}} = \frac{\sqrt{2}L}{F}\,\frac{1}{V_{\rm A,i}}\,(\ell/a)\,\frac{\zeta-1}{\sqrt{\zeta(\zeta+1)}} \ , \qquad (19)$$

where the previously computed expression for the phase speed $v_{\rm ph}$ has been used, and the expression for $\xi_{\rm E}$ from Eq. (2) is inserted. In the remainder of the manuscript we take the measurement length $L = 250$ Mm as in Tomczyk & McIntosh (2009). The factor $\mathbb{T}$ controls the rate of change of the power ratio as a function of frequency. It is a function of the loop parameters ℓ/a, ζ and $V_{\rm A,i}$, which are assumed to be fundamental properties of the observed coronal loops. We wish to constrain the values of these variables through statistical means, only for the specific loops. Note that the value of these variables may differ for other loops (especially $V_{\rm A,i}$) and an over-arching statistical study would have to be conducted using many (currently non-existing) CoMP-like observations to explore statistical constraints on ℓ/a and ζ for all loops, such has been done in Sect. 2. We consider the three variables as independent statistical variables and each of them has a uniform distribution. To the uniform distributions for ℓ/a and ζ, described in Eq. (4), we add a third uniform distribution for $V_{\rm A,i}$:

$$\frac{dV_{\rm A,i}}{dN} \;=\; H(V_{\rm A,i}, V_{\rm A,i,min}, V_{\rm A,i,max}) \;. \tag{20}$$

With these variables, we can calculate the phase speed and power-ratio of the transverse waves using Eqs. (17) and (18). To obtain Fig. 8, we have generated 1000 different loops, and multiplied by a linear function in the frequency domain f to guarantee an even spread across the spectrum. For the sake of simplicity, we have taken the upward/downward ratio $P_{\rm out}/P_{\rm in} = 1$, even though Verth et al. (2010) found $P_{\rm out}/P_{\rm in} = 0.91$ from a fit to the data. A good fit between the data and the statistical loops is obtained for $\ell/a \in [0.5,1]$, $\zeta \in [2.5,4]$ and $V_{\rm A,i} \in [800,1000]$ km/s. These fitting parameters above are not the only ones to yield good results. Other combinations may yield similarly good results.

In Fig. 8, it can be observed that the spread of the statistical points increases with increasing frequency. Also, when $f \to 0$, the spread disappears and the power ratio becomes exactly unity. This is a consequence of the exponential damping by resonant absorption. Indeed, when taking the limit $f \to 0$ in Eq. 19, the argument goes exactly to 0. The increasing spread with increasing frequency can also be understood in similar terms. For the sake of simplicity, let's assume that $\mathbb{T} \sim N(\mu, \sigma^2)$ has a Gaussian distribution with mean μ and spread σ. From elementary statistics, we learn that $\mathbb{T}f \sim N(f\mu, f^2\sigma^2)$, resulting in a larger spread for larger frequencies. Also, the mean will increase linearly with f, which is observed in Fig. 8 as well.

In the end, only the statistical properties of $\mathbb{T}$ determine the fitting with the observed data points. Indeed, one may increase the spread in $V_{\rm A,i}$ by reducing the spread of ℓ/a while keeping the average of their product constant. Likewise, the average Alfvén transit time can be decreased by increasing ℓ/a. Also (as can be seen in Fig. 6), when ζ is increased, the resulting $\mathbb{T}$ is naturally distributed more narrowly, allowing for a wider spread in $V_{\rm A,i}$.

We now take a more statistically rigorous approach. To gain insight on the distribution of $\mathbb{T}$, we calculate the regression of the logarithm of Eq. (18), and we find that

$$<P(f)>_{\rm ratio} = \; b\,{\rm e}^{\mathbb{T}f} \;,\; \ln b = -0.24 \pm 0.17 \;,\; \mathbb{T} = 350 \pm 70\,{\rm s} \;, \tag{21}$$

The uncertainties are calculated using the vertical spread of the residues ($\sigma_{P-P_{\rm fit}} = 0.54$) as an error estimate on the initial measurements and using the method as detailed in Chapter 15.2 of Press et al. (2007). This produces a mean $\mu_{\mathbb{T}} = 350$ s, and standard deviation $\sigma^2_{\mathbb{T}} = 4900$ s^2 of the distribution $\mathbb{T}$. From $\ln b$ = -0.24, we estimate $P_{\rm out}/P_{\rm in} = 0.79$. Verth et al. (2010) had found a larger value of $P_{\rm out}/P_{\rm in} = 0.91$, but as this lies within one sigma of our value, there is statistically no discrepancy.

Let us now consider $\mathbb{T}$ as a statistical distribution, being the product of the independent statistical variables $V_{\rm A,i}$, ℓ/a and $g(\zeta)$=$(\zeta - 1)/\sqrt{\zeta(\zeta+1)}$. Similarly as in Sect. 2, an analytical distribution could be calculated but because $\mathbb{T}$ depends on three statistical variables and the dependency on ζ is more elaborate, this becomes impractical. Instead, we aim to constrain the independent statistical variables using the fit. Since we assume that $V_{\rm A,i}$, ℓ/a and $g(\zeta)$ are independent, it is possible to write

$$\frac{\sqrt{2}}{\pi L}\,\mu_{\mathbb{T}} \;=\; \mu_{1/V_{\rm A,i}}\,\mu_{\ell/a}\,\mu_{g(\zeta)} \;, \tag{22}$$

$$\begin{aligned}\frac{2}{\pi^2 L^2}\,\sigma^2_{\mathbb{T}} \;&=\; (\mu^2_{1/V_{\rm A,i}} + \sigma^2_{\tau_{\rm A,i}})(\mu^2_{\ell/a} + \sigma^2_{\ell/a})(\mu^2_{g(\zeta)} + \sigma^2_{g(\zeta)}) - \mu^2_{1/V_{\rm A,i}}\mu^2_{\ell/a}\mu^2_{g(\zeta)} \\ &=\; \sigma^2_{1/V_{\rm A,i}}\sigma^2_{\ell/a}\sigma^2_{g(\zeta)} + \mu^2_{1/V_{\rm A,i}}\sigma^2_{\ell/a}\sigma^2_{g(\zeta)} + \sigma^2_{1/V_{\rm A,i}}\mu^2_{\ell/a}\sigma^2_{g(\zeta)} \\ &+\; \sigma^2_{1/V_{\rm A,i}}\sigma^2_{\ell/a}\mu^2_{g(\zeta)} + \mu^2_{1/V_{\rm A,i}}\mu^2_{\ell/a}\sigma^2_{g(\zeta)} + \mu^2_{1/V_{\rm A,i}}\sigma^2_{\ell/a}\mu^2_{g(\zeta)} \\ &+\; \sigma^2_{1/V_{\rm A,i}}\mu^2_{\ell/a}\mu^2_{g(\zeta)} \;.\end{aligned} \tag{23}$$

All the terms on the right hand side of Eq. (23) are positive. By considering only the last term and dividing Eq. (23) by the square of Eq. (22), we find

$$0.04 \;=\; \frac{4900}{350^2} \;=\; \left(\frac{\sigma_{\mathbb{T}}}{\mu_{\mathbb{T}}}\right)^2 \;>\; \left(\frac{\sigma_{1/V_{\rm A,i}}}{\mu_{1/V_{\rm A,i}}}\right)^2 \;, \tag{24}$$

because positive terms have been neglected in the right hand side of Eq. (23). Considering only the second and third to last term, we can derive that

$$\left(\frac{\sigma_{\ell/a}}{\mu_{\ell/a}}\right)^2 \;<\; 0.04 \;,\; \left(\frac{\sigma_{g(\zeta)}}{\mu_{g(\zeta)}}\right)^2 \;<\; 0.04 \;, \tag{25}$$

but also

$$\left(\frac{\sigma_{1/V_{\rm A,i}}}{\mu_{1/V_{\rm A,i}}}\right)^2 + \left(\frac{\sigma_{\ell/a}}{\mu_{\ell/a}}\right)^2 + \left(\frac{\sigma_{g(\zeta)}}{\mu_{g(\zeta)}}\right)^2 \;<\; 0.04 \;. \tag{26}$$

These equations prove that the first four terms in Eq. (23) can be neglected compared with the last three terms.

The relations (24)-(25) contain information on the statistical distribution of $V_{\rm A,i}$, ℓ/a and ζ. As we have done in the forward modelling, we shall consider ℓ/a as uniformly distributed $H(\ell/a, (\ell/a)_{\rm min}, (\ell/a)_{\rm max})$. From statistics, we know that for this distribution the mean and variance are equal to $\mu_{\ell/a} = ((\ell/a)_{\rm min} + (\ell/a)_{\rm max})/2$ and $\sigma^2_{\ell/a} = ((\ell/a)_{\rm max} - (\ell/a)_{\rm min})^2/12$, respectively. Using Eq. (24), we find

$$\left(\frac{\sigma_{\ell/a}}{\mu_{\ell/a}}\right)^2 \;=\; \frac{1}{3}\left(\frac{(\ell/a)_{\rm max} - (\ell/a)_{\rm min}}{(\ell/a)_{\rm min} + (\ell/a)_{\rm max}}\right)^2 \;<\; 0.04 \;, \tag{27}$$

or using that $(\ell/a)_{\rm max} > (\ell/a)_{\rm min}$,

$$\begin{aligned}&\frac{(\ell/a)_{\rm max} - (\ell/a)_{\rm min}}{(\ell/a)_{\rm min} + (\ell/a)_{\rm max}} \;<\; \sqrt{0.12} \;\;\Rightarrow \\ &\qquad (\ell/a)_{\rm max} \;<\; \frac{1+\sqrt{0.12}}{1-\sqrt{0.12}}\,(\ell/a)_{\rm min} \;=\; 2.06\,(\ell/a)_{\rm min} \;.\end{aligned} \tag{28}$$

This leaves a rather narrow range for ℓ/a. If it is expected from physical reasons or loop modelling that the inhomogeneity layer covers the whole loop, $(\ell/a)_{\rm max}$=2, then the lower boundary for that length scale is $(\ell/a)_{\rm min} > 0.97$.

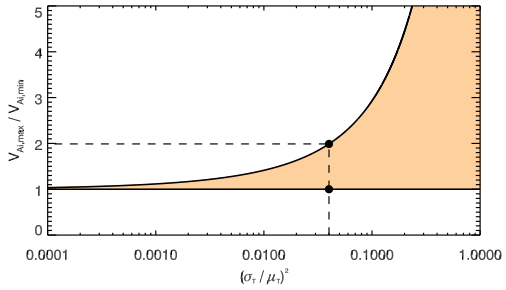

Fig. 9. Uncertainty interval of $V_{\mathrm{A,i,max}}/V_{\mathrm{A,i,min}}$ as a function of the relative variance $(\sigma_{\mathbb{T}}/\mu_{\mathbb{T}})^2$, derived from Eq. (31) The interval given by Eq. (32) for $(\sigma_{\mathbb{T}}/\mu_{\mathbb{T}})^2 = 0.04$ is indicated.

Also assuming a homogeneous distribution of $V_{\mathrm{A,i}}$, we can calculate the mean $\mu_{1/V_{\mathrm{A,i}}}$ (introducing the notation $\Delta V_{\mathrm{A}} = V_{\mathrm{A,i,max}} - V_{\mathrm{A,i,min}}$) as

$$\mu_{1/V_{\mathrm{A,i}}} = E\left[\frac{1}{V_{\mathrm{A,i}}}\right] = \frac{1}{\Delta V_{\mathrm{A}}}\int_{V_{\mathrm{A,i,min}}}^{V_{\mathrm{A,i,max}}}\frac{\mathrm{d}V_{\mathrm{A}}}{V_{\mathrm{A}}} = \frac{1}{\Delta V_{\mathrm{A}}}\ln\left|\frac{V_{\mathrm{A,i,max}}}{V_{\mathrm{A,i,min}}}\right| , \quad (29)$$

where $E[.]$ is the expected value of the argument function. The variance is computed as

$$\sigma^2_{1/V_{\mathrm{A,i}}} = E\left[\frac{1}{V^2_{\mathrm{A,i}}}\right] - E\left[\frac{1}{V_{\mathrm{A,i}}}\right]^2 = \frac{1}{V_{\mathrm{A,i,min}}V_{\mathrm{A,i,max}}} - \mu^2_{1/V_{\mathrm{A,i}}} . \quad (30)$$

Thus, we find the condition for $V_{\mathrm{A,i,min}}$ and $V_{\mathrm{A,i,max}}$:

$$0.04 > \left(\frac{\sigma_{1/V_{\mathrm{A,i}}}}{\mu_{1/V_{\mathrm{A,i}}}}\right)^2 = \frac{(\Delta V_{\mathrm{A}})^2}{V_{\mathrm{A,i,min}}V_{\mathrm{A,i,max}}}\frac{1}{\ln^2\left|\frac{V_{\mathrm{A,i,max}}}{V_{\mathrm{A,i,min}}}\right|} - 1 . \quad (31)$$

This transcendental equation can be solved numerically for $V_{\mathrm{A,i,max}}/V_{\mathrm{A,i,min}}$, and the result is shown in Fig. 9. For $\sigma^2_{\mathbb{T}}/\mu^2_{\mathbb{T}} = 0.04$, we find

$$1 < \frac{V_{\mathrm{A,i,max}}}{V_{\mathrm{A,i,min}}} < 1.9885 , \quad (32)$$

which shows that the loop Alfvén speed is constrained even narrower than ℓ/a.

Interestingly, Tomczyk & McIntosh (2009) found a phase speed of 600 km s^{-1} for the propagating transverse waves. In our current model (i.e. an overdense loop experiencing resonant damping of the waves), this value is an upper limit for the Alfvén speed in the loop: $V_{\mathrm{A,i,max}} = 600$ km s^{-1}. This leads to a minimum value for the Alfvén speed of $V_{\mathrm{A,i,min}} = 300$ km s^{-1}, in order to still be able to explain the small spread in the observed power ratio. Such small values are conceivable since the magnetic field strength in a loop arcade is expected to decrease with loop length. Alfvén speeds in the range of 300-400 km s^{-1} have been reported for loops with lengths larger than 650 Mm (Verwichte et al. 2010).

To find estimates for the distribution of parameter ζ, more effort has to be made, because it occurs through the function $g(\zeta)$. Let us as before assume that ζ is uniformly distributed $H(\zeta, \zeta_{\mathrm{min}}, \zeta_{\mathrm{max}})$. The mean and variance of $g(\zeta)$ can be calculated analytically, see appendix A. Fixing ζ_{min}, we can compute the maximally allowed ζ_{max} to satisfy Eq. (25). The results of this computation are shown in Fig. 10 where contours of constant values of $(\sigma_{g(\zeta)}/\mu_{g(\zeta)})^2$ are shown in the parameter space

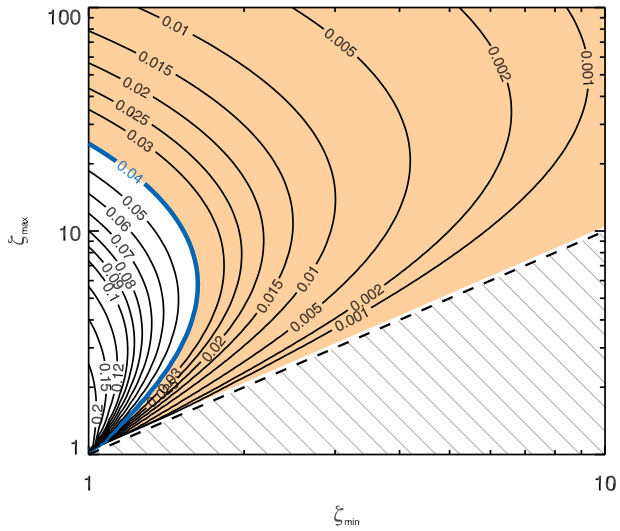

Fig. 10. Contours of constant values of $(\sigma_{g(\zeta)}/\mu_{g(\zeta)})^2$ as a function of ζ_{min} and ζ_{max}. The dashed line is the bisector and the hatched region indicates unphysical values of ζ_{max}. The region in parameter space where $(\sigma_{g(\zeta)}/\mu_{g(\zeta)})^2 < 0.04$ is shaded.

ζ_{min}-ζ_{max}. For $(\sigma_{\mathbb{T}}/\mu_{\mathbb{T}})^2 = 0.04$, the valid range of values of ζ_{min} and ζ_{max} that are consistent with the observations are indicated as a shaded region. The smaller the error in $\mathbb{T}$, the smaller the admissible region becomes (i.e. contours for smaller ratios are more to the right). For all values of the error and ζ_{min}, $\zeta_{\mathrm{max}} \to \infty$ is not excluded and thus ζ is never constrained. However, realistically, we can assume a reasonable finite upper limit for ζ of order 10 (e.g. from loop physics it is known that the density contrast $\zeta \leq 10$). Then we see that ζ_{max} can become even more constrained for small values of ζ_{min} as long as the error in $\mathbb{T}$ is small enough such that the contour of this error remains above this upper limit at the left axis $\zeta_{\mathrm{min}} = 1$ (e.g. for $\zeta \leq 10$, if $(\sigma_{\mathbb{T}}/\mu_{\mathbb{T}})^2$ <0.08 a much stronger upper limit for ζ may be found). For $(\sigma_{\mathbb{T}}/\mu_{\mathbb{T}})^2 = 0.04$ there is a restricted range of ζ for $\zeta_{\mathrm{min}} < 1.63$. $\zeta_{\mathrm{min}} = 1.63$ is the maximal extent of the contour because of the asymptotic behaviour of $g(\zeta)$ (see Fig. 6). If ζ_{min} is increased beyond this value, no ζ_{max} can be excluded, and no statements can be made on the statistical distribution of ζ.

The external Alfvén speed, $V_{\mathrm{A,e}}$, is constrained to be within the interval

$$\max\left\{v_{\mathrm{ph}}, \sqrt{\zeta_{\mathrm{min}}}\,V_{\mathrm{A,i,min}}\right\} < V_{\mathrm{A,e}} < \sqrt{\zeta_{\mathrm{max}}}\,V_{\mathrm{A,i,max}} . \quad (33)$$

For a fixed value of $\sigma_{\mathbb{T}}/\mu_{\mathbb{T}}$, using Eq. (31) and taking $v_{\mathrm{ph}} = V_{\mathrm{A,i,min}}$, the ratio $(V_{\mathrm{A,e}}/V_{\mathrm{A,i,min}})^2$ is determined by ζ_{min}, i.e.

$$\max\left\{\left(\frac{V_{\mathrm{A,i,max}}}{V_{\mathrm{A,i,min}}}\right)^2, \zeta_{\mathrm{min}}\right\} < \left(\frac{V_{\mathrm{A,e}}}{V_{\mathrm{A,i,min}}}\right)^2 < \left(\frac{V_{\mathrm{A,i,max}}}{V_{\mathrm{A,i,min}}}\right)^2_{\mathrm{max}}\zeta_{\mathrm{max}} . \quad (34)$$

We may employ again Fig. 10 to determine the interval of admissible values. For $(\sigma_{\mathbb{T}}/\mu_{\mathbb{T}})^2 = 0.04$, $\max(V_{\mathrm{A,i,max}}/V_{\mathrm{A,i,min}}) = 1.9885$ and $V_{\mathrm{A,i,max}} = 600$ km s^{-1}, we find the following constraints for $V_{\mathrm{A,e}}$. For $\zeta_{\mathrm{min}} = 1$, $V_{\mathrm{A,e}}$ is constrained to be exactly equal to $V_{\mathrm{A,i,max}}$. For increasing ζ_{min}, the upper bound increases until for $\zeta_{\mathrm{min}} = 1.63$ the interval becomes 600 km s^{-1} < $V_{\mathrm{A,e}}$ < 800 km s^{-1}. For $1.63 < \zeta_{\mathrm{min}} \leq 3.95$, $V_{\mathrm{A,e}}$ is only constrained to be larger than 600 km s^{-1}. For $\zeta_{\mathrm{min}} > 3.95$, the lower bound needs to be larger than $\sqrt{\zeta_{\mathrm{min}}}$ 300 km s^{-1}.

4. Conclusions

We have explored how through a statistical approach coronal loop cross-sectional characteristics such as density contrast and transition layer width can be seismologically constrained using observations of transverse waves and oscillations.

We have investigated transverse loop oscillations, the majority of which have been observed by TRACE and SDO. First, we have produced through forward-modelling many observed realisations of TLOs periods and damping times from sampled values of ℓ/a and ζ. The index of the power law fit follows a Gaussian distribution centred on an index value of one. The uncertainty (Gaussian width) of the index strongly depends on the range of periods used. For a range of periods between 140 and 440s, as seen by Aschwanden et al. (2002), the uncertainty becomes as large as 0.5. But for a period between 50 and 3600 s, the uncertainty is only 0.14. We have demonstrated that the observed period-damping time scaling law does provide information about the physical damping mechanism, provided observations of TLOs are collected from as wide as possible range of periods and provided a comparison with theory is performed in a statistical sense. Importantly, we have assumed that the distributions of these two parameters from which we sample is the same for all periods (and hence also loop length). We have not taken into account the possibility of different classes of coronal loops present within the observations. We are confident that this is a reasonable assumption because most reported TLOs come from similarly sized active region loops. Without this assumption and the observed TLOs would somehow have widely different cross-sectional structuring that also depends on period, than almost any power law may be expected (Arregui et al. 2008).

With the full range of values for ℓ/a and $\zeta_{\rm min}$=1, we find the best fit as a function of the one remaining free parameter, $\zeta_{\rm max}$, equal to 3. However, the error in both the observational and the forward-modelling of the value of α is large. Instead, to increase statistics, we have reduced the problem to a one-dimensional distribution of the quality factor τ/P. For given distribution of ℓ/a and ζ we have calculated the shape of the quality factor distribution. As already noted by Goossens et al. (2008), τ/P has a minimum value determined by $(\ell/a)_{\rm max}$ and $\zeta_{\rm max}$. Fitting the observed quality-factor distribution of TLOs showed that loops with large values of ℓ/a and ζ are not consistent with the observations. It is important to note that such loops would support transverse oscillations with a poor quality-factor, whose transverse oscillations for typical displacement amplitudes and periods would be difficult to detect. There is an observer bias against studying such loops. Therefore, instead of relying only on the lower limit of observed quality factor to constrain ℓ/a and ζ, we determine it by fitting the distribution curve to all observations, and find $(\tau/P)_{\rm min} = 0.65$. From the resulting relation between $\zeta_{\rm max}$ and $(\ell/a)_{\rm max}$, we see that the density contrast is only constrained if $(\ell/a)_{\rm max}$ is larger than 0.98, and that $\zeta_{\rm max}$ decreases as a function of $(\ell/a)_{\rm max}$ until a value of approximately 3 for $(\ell/a)_{\rm max} = 2$. The latter value is broadly consistent with the scaling law fitting. Loops with simultaneously large values of ℓ/a and ζ, i.e. smooth and large contrasted loops, are inconsistent with the observations. In interpreting these results we need to bear in mind that the analytical resonant absorption equation is strictly speaking valid only for small values of ℓ/a. This study could be repeated using numerical solutions of the resonant absorption problem, which allows for an arbitrary transition layer thickness (e.g. Van Doorsselaere et al. 2004).

For the CoMP running transverse waves, we have reproduced the observed power ratio dependency with the frequency, using uniform distributions for ℓ/a, $V_{\rm A,i}$ and ζ (as for the TLOs). In the forward modelling, it became obvious that relatively narrow ranges had to be used in order to fit the observed spread on the data points. Taking a more statistically rigorous approach, we have studied the mean and the spread on the parameter $\mathbb{T}$. This parameter contains all the statistical information of the loop. From the fitted values and spread of $\mathbb{T}$, it was possible to constrain the distributions of ℓ/a, $V_{\rm A,i}$ and ζ. It was found that the ratio of upper and lower bounds on the uniform distribution of ℓ/a and $\tau_{\rm A,i}$ should be less than 2.06, to comply with the statistical properties of $\mathbb{T}$. Additionally, the distribution for the loop density contrast could be either extremely narrow, or wide. Depending on other physical estimates for upper limits of the density contrast, a severe restriction could be found for the density contrast distribution. A similar analysis could not be made for the TLOs because the uncertainty on the fit parameter is too large.

The statistical study of TLOs permits to determine constraints on the physical characteristics of coronal loops as a whole. One of the main unanswered questions surrounding coronal wave dynamics is the selective (degree of) excitation of loops in active regions. It is possible that the physical mechanisms that excite these oscillations, e.g. shocks, heating, pressure imbalance, are selective in for example direction or distance. But another possible explanation may be formulated from the result of $(\tau/P)_{\rm min}$. It reveals that some loops may not be seen (reported) to oscillate transversely because they have oscillations with a quality factor too small to be detected as an oscillation by an observer. The CoMP study reveals narrow distributions for the statistical parameters suggest that all loops observed with CoMP have similar properties. A rather narrow distribution for loop density contrast is found. Perhaps our result is the consequence of only studying one time series in one active region but it may also reveal a strong constraint on the understanding and modelling of loop physics. Are the oscillating loops a special subset of the large ensemble of coronal loops, or do all loops have e.g. a density contrast in a small range?

To decrease the uncertainties we need many more observations of standing and running transverse waves in as wide a range of active regions/temperatures and periods as possible. The characterisation of TLOs is a labour-intensive data-analysis process because of the need for the detection of transverse displacements in images. Systematic and consistent methods of analysis of TLOs are being developed (Verwichte et al. 2009, 2010; White & Verwichte 2012). A much larger set of observations would allow us to explore the existence of different sub-classes of coronal loops, possibly linked to specific regions. Also, it would require further coronal loop modelling and observational studies of non-oscillating loops.

Acknowledgements

EV acknowledges financial support from the UK Science and Technology Facilities Council (STFC) on the CFSA Rolling Grant and the SF fellowship of the KU Leuven Research Council with number SF/12/004, TVD and PA have received funding from the Odysseus programme of the FWO-Vlaanderen. TVD also acknowledges funding from the EU's Framework Programme 7 as an ERG with grant number 276808. RSW would like to acknowledge the support of an STFC Ph.D. studentship.

References

Arregui, I., Andries, J., Van Doorsselaere, T., Goossens, M., & Poedts, S. 2007, A&A, 463, 333

Arregui, I. & Asensio Ramos, A. 2011, ApJ, 740, 44

Arregui, I., Ballester, J. L., & Goossens, M. 2008, ApJ, 676, L77
Aschwanden, M. J., de Pontieu, B., Schrijver, C. J., & Title, A. M. 2002, Sol. Phys., 206, 99
Aschwanden, M. J., Fletcher, L., Schrijver, C. J., & Alexander, D. 1999, ApJ, 520, 880
Aschwanden, M. J., Nightingale, R. W., Andries, J., Goossens, M., & Van Doorsselaere, T. 2003, ApJ, 598, 1375
De Moortel, I. & Brady, C. S. 2007, ApJ, 664, 1210
Edwin, P. M. & Roberts, B. 1983, Sol. Phys., 88, 179
Goossens, M., Andries, J., & Aschwanden, M. J. 2002, A&A, 394, L39
Goossens, M., Andries, J., Soler, R., et al. 2012, ApJ, 753, 111
Goossens, M., Arregui, I., Ballester, J. L., & Wang, T. J. 2008, A&A, 484, 851
Goossens, M., Hollweg, J. V., & Sakurai, T. 1992, Sol. Phys., 138, 233
Handy, B. N., Acton, L. W., Kankelborg, C. C., et al. 1999, Sol. Phys., 187, 229
Hollweg, J. V. & Yang, G. 1988, J. Geophys. Res., 93, 5423
Hori, K., Ichimoto, K., & Sakurai, T. 2007, in Astronomical Society of the Pacific Conference Series, Vol. 369, New Solar Physics with Solar-B Mission, ed. K. Shibata, S. Nagata, & T. Sakurai, 213
Hori, K., Ichimoto, K., Sakurai, T., Sano, I., & Nishino, Y. 2005, ApJ, 618, 1001
Howard, R. A., Moses, J. D., Vourlidas, A., et al. 2008, Space Sci. Rev., 136, 67
Ionson, J. A. 1978, ApJ, 226, 650
Lemen, J. R., Title, A. M., Akin, D. J., et al. 2012, Sol. Phys., 275, 17
McIntosh, S. W., de Pontieu, B., Carlsson, M., et al. 2011, Nature, 475, 477
McIntosh, S. W., de Pontieu, B., & Tomczyk, S. 2008, Sol. Phys., 252, 321
Mrozek, T. 2011, Sol. Phys., 270, 191
Nakariakov, V. M. & Ofman, L. 2001, A&A, 372, L53
Nakariakov, V. M., Ofman, L., Deluca, E. E., Roberts, B., & Davila, J. M. 1999, Science, 285, 862
Ofman, L. & Aschwanden, M. J. 2002, ApJ, 576, L153
Pascoe, D. J., Hood, A. W., de Moortel, I., & Wright, A. N. 2012, A&A, 539, A37
Press, W. H., Teukolsky, S. A., Vetterling, W. T., & Flannery, B. P. 2007, Numerical Recipes: The Art of Scientific Computing
Ruderman, M. S. & Roberts, B. 2002, ApJ, 577, 475
Schmelz, J. T., Beene, J. E., Nasraoui, K., et al. 2003, ApJ, 599, 604
Terradas, J., Goossens, M., & Verth, G. 2010, A&A, 524, A23
Terzo, S. & Reale, F. 2010, A&A, 515, A7
Tomczyk, S., Card, G. L., Darnell, T., et al. 2008, Sol. Phys., 247, 411
Tomczyk, S. & McIntosh, S. W. 2009, ApJ, 697, 1384
Tomczyk, S., McIntosh, S. W., Keil, S. L., et al. 2007, Science, 317, 1192
Van Doorsselaere, T., Andries, J., Poedts, S., & Goossens, M. 2004, ApJ, 606, 1223
Van Doorsselaere, T., Birtill, D. C. C., & Evans, G. R. 2009, A&A, 508, 1485
Van Doorsselaere, T., Nakariakov, V. M., & Verwichte, E. 2007, A&A, 473, 959
Verth, G., Terradas, J., & Goossens, M. 2010, ApJ, 718, L102
Verwichte, E., Aschwanden, M. J., Van Doorsselaere, T., Foullon, C., & Nakariakov, V. M. 2009, ApJ, 698, 397
Verwichte, E., Foullon, C., & Nakariakov, V. M. 2006, A&A, 452, 615
Verwichte, E., Foullon, C., & Van Doorsselaere, T. 2010, ApJ, 717, 458
Verwichte, E., Nakariakov, V. M., Ofman, L., & Deluca, E. E. 2004, Sol. Phys., 223, 77
Verwichte, E., Van Doorsselaere, T., White, R., Bacon, A., & Williams, A. 2012, A&A
Wang, T., Ofman, L., Davila, J. M., & Su, Y. 2012, ApJ, 751, L27
Wang, T. J. & Solanki, S. K. 2004, A&A, 421, L33
Wentzel, D. G. 1979, ApJ, 227, 319
White, R. S. & Verwichte, E. 2012, A&A, 537, A49
White, R. S., Verwichte, E., & Foullon, C. 2012, A&A, 545, A129

Appendix A: Mean and variance of $g(\zeta)$

For ζ uniformly distributed $H(\zeta, \zeta_{\min}, \zeta_{\max})$, the mean and variance of $g(\zeta)$ can be calculated analytically. The mean is found (introducing the notation $\Delta\zeta = \zeta_{\max} - \zeta_{\min}$),

$$\begin{aligned}\mu_{g(\zeta)} &= \frac{1}{\Delta\zeta}\int_{\zeta_{\min}}^{\zeta_{\max}} g(\zeta)\,\mathrm{d}\zeta\ ,\\ &= \frac{1}{\Delta\zeta}\int_{\zeta_{\min}}^{\zeta_{\max}} \frac{\zeta-1}{\sqrt{\zeta(\zeta+1)}}\,\mathrm{d}\zeta\ ,\\ &= \frac{1}{\Delta\zeta}\left[\sqrt{\zeta\,(\zeta+1)} - 3\mathrm{arcsinh}(\sqrt{\zeta})\right]_{\zeta_{\min}}^{\zeta_{\max}}\ . \end{aligned} \tag{A.1}$$

The variance can be calculated through

$$\sigma^2_{g(\zeta)} = E[g^2] - (E[g])^2 = E[g^2] - \mu^2_{g(\zeta)}\ , \tag{A.2}$$

where $E[.]$ stands for the expected value of the argument function. For $g(\zeta)$, we find

$$\begin{aligned}E[g^2] &= \frac{1}{\Delta\zeta}\int_{\zeta_{\min}}^{\zeta_{\max}} g^2(\zeta)\,\mathrm{d}\zeta\ ,\\ &= \frac{1}{\Delta\zeta}\int_{\zeta_{\min}}^{\zeta_{\max}} \frac{(\zeta-1)^2}{\zeta(\zeta+1)}\,\mathrm{d}\zeta\ ,\\ &= \frac{1}{\Delta\zeta}\left[\zeta + \ln(\zeta) - 4\ln(\zeta+1)\right]_{\zeta_{\min}}^{\zeta_{\max}}\ , \end{aligned} \tag{A.3}$$

which is combined with Eq. (A.1) to compute Eq. (A.2).